# OMNIDIRECTIONAL THERMAL ANEMOMETER FOR LOW AIRSPEED AND MULTI-POINT MEASUREMENT APPLICATIONS

Y. Gao[a,b], B. C. Ramirez[a], and S. J. Hoff[a]

[a] Department of Agricultural and Biosystems Engineering, Iowa State University, Ames, IA, USA

[b] College of Engineering, Huazhong Agricultural University and the Cooperative Innovation Center for Sustainable Pig Production, Wuhan, China

**Corresponding author:** Brett C. Ramirez, 4332B Elings Hall, Department of Agricultural and Biosystems Engineering, Iowa State University, Ames, IA, USA; phone: 815-353-8299; e-mail: bramirez@iastate.edu.

**Abstract.** Current control strategies for livestock and poultry facilities need to improve their interpretation of the Thermal Environment (TE) that the animals are experiencing in order to provide an optimum TE that is uniformly distributed throughout the facility; hence, airspeed, a critical parameter influencing evaporative and convective heat exchange must be measured. An omnidirectional, constant temperature, thermal anemometer (TA) with ambient dry-bulb temperature ($t_{db}$) compensation was designed and developed for measuring airspeeds between 0 and 6.0 m $s^{-1}$. An Arduino measured two analog voltages to determine the thermistor temperature and subsequently the power being dissipated from a near-spherical overheated thermistor in a bridge circuit with a transistor and operational amplifier. A custom wind tunnel featuring a 0.1 m diameter pipe with an access for TA insertion was constructed to calibrate the TA at different temperatures and airspeeds, at a constant relative humidity. The heat dissipation factor was

calculated for a given airspeed at different ambient temperatures ranging from 18°C to 34°C and used in a unique fourth-order polynomial regression that compensates for temperature using the fluid properties evaluated at the film temperature. A detailed uncertainty analysis was performed on all key measurement inputs, such as the microcontroller analog to digital converter, TA and $t_{db}$ thermistor regression statistics, and the calibration standard, that were propagated through the calibration regression. Absolute combined standard uncertainty associated with temperature corrected airspeed measurements ranged from 0.11 m $s^{-1}$ (at 0.47 m $s^{-1}$; 30.3% relative) to 0.71 m $s^{-1}$ (at 5.52 m $s^{-1}$; 12.8% relative). The TA system cost less than $35 USD in components and due to the simple hardware, this thermal anemometer is well-suited for integration into multi-point data acquisition systems analyzing spatial and temporal variability inside livestock and poultry housing.

**Keywords.** air velocity, convection, livestock, poultry, thermal environment, and uncertainty.

**Graphical Abstract.**

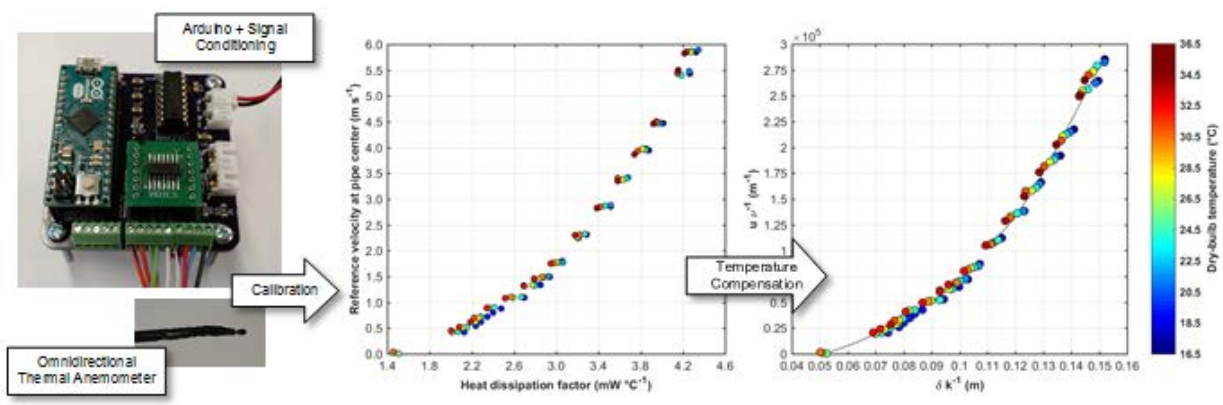


**Highlights.**

- An anemometer system was developed for multipoint measurements in livestock housing
- Extensive uncertainty analysis was performed through entire measurement process
- Suitable performance for low airspeed measurements at temperatures in animal housing
- Inexpensive discretized assessment of thermal environment of livestock is possible

**Nomenclature.**

| | |
|---|---|
| AOZ | Animal Occupied Zone |
| TE | Thermal Environment |
| TA | Thermal Anemometer |
| LVTA | Low Velocity Thermal Anemometer |
| DAQ | Data Acquisition |
| ADC | Analog to Digital Converter |
| RH | Relative Humidity (%) |
| $P$ | Power (W) |
| $\delta$ | heat dissipation factor (W °C$^{-1}$) |
| $t_{db}$ | dry-bulb temperature (°C) |
| $t_t$ | thermal anemometer thermistor temperature (°C) |
| $h$ | convective heat transfer coefficient (W °C$^{-1}$ m$^{-2}$) |
| $A_t$ | thermal anemometer thermistor surface area (m$^2$) |
| $Nu$ | Nusselt Number (dimensionless) |
| $k$ | thermal conductivity at film temperature (W °C$^{-1}$ m$^{-1}$) |
| $d_t$ | thermal anemometer thermistor diameter (m) |
| $f$ | functional dependence |
| $Re$ | Reynold's number (dimensionless) |
| $u$ | airspeed (m s$^{-1}$) |
| $v$ | kinematic viscosity (m$^2$ s$^{-1}$) |
| NTC | Negative Temperature Coefficient |
| CTA | Constant Temperature Anemometer |
| $I_t$ | current through the thermal anemometer thermistor (A) |
| $V_s$ | supply voltage ($V_{DC}$) |
| $V_1$ | noninverting terminal voltage ($V_{DC}$) |
| $R_x$ | resistance value at location x (Ω) |
| $V_2$ | emitter voltage ($V_{DC}$) |
| $R_t$ | thermistor resistance (Ω) |
| $V_{db}$ | ambient $t_{db}$ divider voltage ($V_{DC}$) |
| $u(t)$ | airspeed as a function of time (m s$^{-1}$) |
| $u_0$ | initial u at time $t_0$ (m s$^{-1}$) |
| $\Delta u$ | difference between $u_0$ and u at steady-state (m s$^{-1}$) |
| $t$ | time (s) |
| $t_0$ | initial time (s) |
| $\tau$ | time constant (s$^{-1}$) |
| $u(t)$ | airspeed as a function of time (m s$^{-1}$) |
| $T_t$ | thermal anemometer thermistor temperature (K) |
| $a_1$-$a_4$ | thermistor temperature regression coefficients |
| $\Delta$ | combined standard uncertainty associated with a parameter |
| $\Delta\bar{V}_j$ | mean analog voltage combined standard uncertainty ($V_{DC}$) |
| $\Delta V_j$ | analog voltage combined standard uncertainty ($V_{DC}$) |
| $SE$ | standard error of the mean measured analog voltages ($V_{DC}$) |
| $\Delta R_t$ | thermal anemometer thermistor resistance combined standard uncertainty (Ω) |
| $\Delta R_x$ | resistor x standard uncertainty (Ω) |
| $n$ | number of data |
| $RMSE$ | Root-Mean-Square Error (dependent variable units) |

| | |
|---|---|
| $y_i$ | dependent variable |
| $\hat{y}_i$ | predicted value from the regression |
| $\Delta t_t$ | thermal anemometer thermistor temperature combined standard uncertainty (°C) |
| $ACC$ | manufacturer's accuracy (°C) |
| $T_{db}$ | $t_{db}$ thermistor temperature (K) |
| $R_{db}$ | thermistor resistance (Ω) |
| $b_1$-$b_4$ | $t_{db}$ thermistor temperature regression coefficients |
| $\Delta t_{db}$ | dry-bulb temperature combined standard uncertainty (°C) |
| $u_{ref}$ | reference airspeed at center of pipe (m $s^{-1}$) |
| $\Delta u_{ref}$ | combined standard sensor (reference) uncertainty (m $s^{-1}$) |
| $dP$ | precision nozzle differential static pressure (Pa) |
| $\Delta dP$ | combined standard sensor (pressure) uncertainty (Pa) |
| $c_1$-$c_4$ | reference airspeed regression coefficients |
| $\Delta u'_{ref}$ | reference airspeed combined standard uncertainty (m $s^{-1}$) |
| $\Delta\delta$ | heat dissipation factor combined standard uncertainty (W °$C^{-1}$) |
| $u'$ | predicted airspeed with $t_{db}$ compensation (m $s^{-1}$) |
| $d_1$ - $d_4$ | predicted airspeed regression coefficients (m $s^{-1}$) |
| $\Delta u'$ | predicted airspeed combined standard uncertainty (m $s^{-1}$) |

# 1 Introduction

The Animal Occupied Zone (AOZ) Thermal Environment (TE) inside livestock and poultry facilities places the animal at risk for adverse health effects and influences animal well-being, growth performance, and feed conversion efficiency (Curtis, 1983; Hillman, 2009; Mount, 1975; Straw, Zimmerman, D'Allaire, & Taylor, 1999). Further, due to the large variability in spatial and temporal distribution of TE (Jerez, Wang, & Zhang, 2014; Zhang, Barber, & Ogilvie, 1988), accurate quantification of AOZ TE by a robust data acquisition system is needed, such that the most effective management strategies and facility designs can be implemented.

The TE describes the parameters that influence heat exchange (i.e., convective, conductive, radiative, and evaporative) between an animal and its surroundings (ASHRAE, 2013; Curtis, 1983; DeShazer, Hahn, & Xin, 2009). Convection is an important mode of heat transfer for animals in housed environments that are driven by ambient dry-bulb temperature ($t_{db}$) and airspeed, with typically only $t_{db}$ used to quantitatively describe and control TE. In a hot ambient $t_{db}$, airspeed is beneficial (i.e., when $t_{db}$ is lower than skin temperature) to the animal because energy generated internally can be more readily released preserving the animal's body temperature; however, convective heat loss decreases as airspeed increases, limiting the effectiveness of high airspeeds. Desired hot ambient $t_{db}$ AOZ airspeeds in facilities are generally up to 3 m $s^{-1}$ (590 ft $min^{-1}$). Conversely, animals in a cold ambient $t_{db}$ prefer low airspeeds (i.e., less than 0.5 m $s^{-1}$) to minimize energy expenditures and avoid drafts that can negatively affect animal performance and health. Therefore, an anemometer is needed to accurately quantify low airspeeds in the AOZ. Heber and Boon (1993) and Luck et al. (2014) have used commercially available anemometers to characterize air velocity distribution and satisfy their research objectives but, lack customization for controller feed-back use and cost effective for widespread use. Measurement of all parameters in the TE

would provide control systems and producers with information about the TE that an animal is directly experiencing, such that design and control of TE modification systems can be adjusted to enhance and maintain the optimal TE for enhanced production efficiency and thermal comfort.

Numerous omnidirectional (e.g., ultrasonic, spherical thermal, and laser-based) and unidirectional (e.g., paddlewheel, three-cup, hot-wire, Pitot tube, and vane) anemometer technologies are commercially available and summarized in literature (ASHRAE, 2013). For the anticipated low airspeeds in livestock and poultry facilities, paddlewheel, three-cup, and vane anemometers are ineffective due to shaft friction. While commercially available ultrasonic and laser-based anemometers are accurate at low airspeeds and provide flow field direction, they are cost prohibitive for multi-point measurement applications. Thermal anemometers (i.e., hot-wire or hot-film) are advantageous due to their cost effectiveness, small size (minimal intrusion in the AOZ), omnidirectional capability, and measurement range (ASHRAE, 2013). A hot-wire anemometer, typically a cylindrical wire is unidirectional (non-isotropic heat loss), can be made omnidirectional, if the wire is replaced with a spherical element. In general, Low Velocity Thermal Anemometers (LVTAs) consist of an element (e.g., thermistor, resistance temperature detector, or thermocouple junction) electrically heated above ambient $t_{db}$. LVTAs maintain either a constant current, constant voltage, or constant temperature at the element (ASHRAE, 2013). Many circuit designs and conditioning methods exist (Bruun, 1996); however, they lack the robustness required for agricultural applications (e.g., durability, customization, etc.) and cost effectiveness for integration into multi-point measurement Data Acquisition (DAQ) systems using inexpensive, open source microcontrollers.

In addition to the transducer, thermal anemometers also require a statement of measurement uncertainty that encompasses the propagation of measurement error through sensor hardware,

airspeed calculation, calibration, temperature compensation, frequency response, and direction sensitivity (Popiolek, Jørgensen, Melikov, Silva, & Kierat, 2007). Framework for performing this uncertainty analysis was established by Popiolek et al. (2007), using a commercially available, omnidirectional LVTA. While this empirical and theoretical analysis exhaustively quantified many key sources of measurement error, analog to digital converter (ADC) error and subsequent transformation to airspeed (by curve-fitting algorithm) were reported by the manufacturer. Variability in thermistor shape and size due to manufacturing is an additional uncertainty source specific to custom developed LVTAs, and is also unknown for commercial LVTAs. Many novel calibration methods for controlling low velocities exist; such as, mounting a LVTA to the end of a swinging arm or pendulum (Al-Garni, 2007; Barfield & Henson, 1971), draining water from a sealed vessel to draw air through a nozzle (Barfield & Henson, 1971; Christman & Podzimek, 1981; Yue & Malmström, 1998), and recording the time required to traverse a measured length (Aydin & Leutheusser, 1980). These diverse and custom approaches to calibration demonstrate that many techniques are plausible, when documented and accompanied with an uncertainty analysis. Likewise, specifically for LVTAs, additional uncertainty is introduced when ambient $t_{db}$ differs from that at calibration; thus, LVTA measurements require compensation for $t_{db}$ (Bruun, 1996). Several theoretical heat transfer based relations and empirical methods through calibration have been developed for $t_{db}$ compensation (Hultmark & Smits, 2010). A simple $t_{db}$ correction method based on calibration data and not theoretical heat transfer law, was applied to airspeeds greater than 3.5 m $s^{-1}$ and $t_{db}$ greater than 33°C for a hot-wire anemometer (Hultmark & Smits, 2010). Little is known about that application of this $t_{db}$ correction method to omnidirectional, constant temperature LVTAs at typical temperatures encountered in livestock housing.

A low-cost, microcontroller-based omnidirectional thermal anemometer, with a well-

documented statement of measurement uncertainty was developed to be integrated into a custom TE sensor array (TESA) that measures $t_{db}$, relative humidity (RH), mean radiant temperature, and airspeed. This novel network of TESAs would provide the capability to study TE spatial and temporal distribution in livestock and poultry facilities with sufficient measurement density. In addition, incorporation of airspeed measurement into ventilation and heat stress alleviation (e.g., sprinklers) control strategies would allow for intelligent TE management decisions that promote the optimum TE for animal to dissipate internally generated heat required for homeothermic balance. Hence, the objectives of this research were: (1) design an economic, omnidirectional thermal anemometer applicable to low airspeed measurements commonly found in livestock and poultry housing; (2) document the calibration standard, procedure, and ambient $t_{db}$ correction method; and (3) quantify the combined standard uncertainty associated with $t_{db}$ compensated airspeed measurements.

# 2 Materials and Methods

## 2.1 Theory of Operation

The steady-state energy balance for a Thermal Anemometer (TA) thermistor element heated above ambient $t_{db}$ (equation 1) has been previously derived in literature.

$$P = \delta\,(t_t - t_{db}) \tag{1}$$

where

| | |
|---|---|
| $P$ | = electrical power (W) |
| $\delta$ | = heat dissipation factor (W °C$^{-1}$) |
| $t_t$ | = thermal anemometer thermistor temperature (°C) |
| $t_{db}$ | = ambient dry-bulb temperature (°C) |

Power required by an electrical source to maintain the element at a constant temperature above ambient $t_{db}$ is a function of the heat dissipation factor ($\delta$) and the temperature difference between the element surface and ambient. Specific to each thermistor, $\delta$ depends on surrounding fluid speed, fluid properties (i.e., specific volume, thermal conductively, kinematic viscosity, etc.), and

relative thermistor orientation in the flow field. For a spherical thermistor in uncompressed air, under a narrow range of ambient $t_{db}$ such that the air properties do not vary greatly, $\delta$ between the thermistor and surrounding air is assumed solely a function of airspeed. Hence, at the steady-state condition, supplied electrical power equals convective heat losses (equation 2).

$$P = h\, A_t\, (t_t - t_{db}) \tag{2}$$

where

| | |
|---|---|
| $h$ | = convective heat transfer coefficient (W °C $^{-1}$ m$^{-2}$) |
| $A_t$ | = thermal anemometer thermistor surface area (m$^2$) |

The convective heat transfer coefficient ($h$) is determined from the thermodynamic properties of the fluid and the relationship between heat transfer and flow around a sphere. The Nusselt number ($Nu$; a function of Reynolds and Prandtl numbers) describes $h$, thermistor diameter, and fluid thermal conductivity relationship. After simplification, $\delta$ can be expressed as function of convective heat losses (equation 3).

$$\delta = \frac{Nu\, k}{d_t}\, A_t \tag{3}$$

where

| | |
|---|---|
| $Nu$ | = Nusselt number (dimensionless) |
| $k$ | = thermal conductivity at film temperature (W m$^{-1}$ °C $^{-1}$) |
| $d_t$ | = thermal anemometer thermistor diameter (m) |

Nusselt numbers for small, spherical thermistor elements have been previously studied and vary greatly in literature (Collis & Williams, 1959; Mori, Imabayashi, Hijikata, & Yoshida, 1968; Rumyantsev & Kharyukov, 2011; Skinner & Lambert, 2009). In addition, accurate measurement of thermistor diameter is difficult; therefore, rather than finding an analytical solution to Nusselt number, a method not based on heat transfer law, but rather the empirical relation between $\delta$ and $t_{db}$ using the properties of the free-stream fluid (i.e., kinematic viscosity and thermal conductivity) evaluated at the film temperature was proposed by Hultmark & Smits (2010; equation 4).

$$\delta \approx f(Re)\frac{k\, A_t}{d_t} \tag{4}$$

where

$f$ = functional dependence

$Re$ = Reynold's number (dimensionless)

The Prandtl number is assumed constant over a narrow ambient $t_{db}$ range; thus, Nusselt number is assumed as only a function of Reynolds number (*Re*). Since thermistor area and diameter are constant, equation 4 can be further simplified (equation 5).

$$\frac{u}{\nu} \approx f\left(\frac{\delta}{k}\right) \tag{5}$$

where

$u$ = airspeed (m $s^{-1}$)

$\nu$ = kinematic viscosity ($m^2$ $s^{-1}$)

While the general form of this relationship has been previously derived (Hultmark & Smits, 2010), experimental results were used to determine the functional dependence between $u\ \nu^{-1}$ and $\delta\ k^{-1}$, which is specific to the thermistor size and shape, $t_{db}$ range, and airspeed range. Absolute viscosity is found using the Sutherland correction (Fox, McDonald, & Pritchard, 1985). Also, thermal conductivity can be determined by the correlation presented by Kannuluik & Carman, (1951), and moist air density calculated by the psychrometric equations (ASHRAE, 2013).

## 2.2 Sensor Module

### 2.2.1 Hardware

A spherical, Negative Temperature Coefficient (NTC) thermistor (nominal 470 Ω at 25°C, Model LC471F3K, U.S. Sensor Corp., Orange, CA, USA) was heated above ambient $t_{db}$ by a Constant Temperature Anemometer (CTA) circuit (figure 1) based on Schiretz (2012). Convective heat transfer was assumed isotropic; however, full omnidirectional sensing was limited by a small conical region due to the attached lead wires. The CTA circuit consisted of a Wheatstone bridge, four channel differential comparator operational amplifier (TLV2434, Texas Instruments Inc., Dallas, TX, USA), and a NPN transistor (2N2222A, Central Semiconductor Corp., Hauppauge,

NY, USA). Analog voltages at $V_1$ and $V_2$ (figure 1) were passed through a voltage follower (not shown) using two of the remaining channels on the operational amplifier prior to measurement with the 10-bit ADC on the microcontroller (Micro, Arduino LLC, Italy).

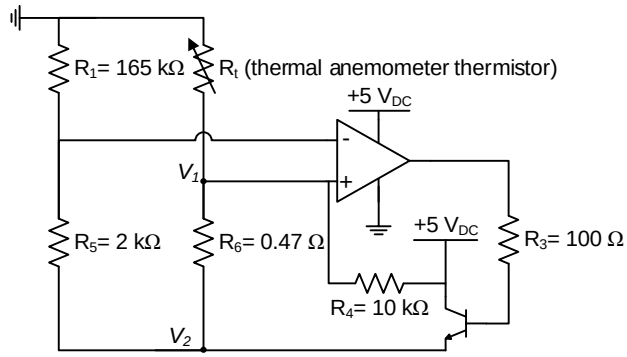


**Figure 1. Constant temperature thermal anemometer circuit based on Schiretz (2012). Analog voltages measured at $V_1$ and $V_2$ were used to determine thermistor temperature and power dissipated.**

In the Wheatstone bridge (figure 1), the three constant resistors and the one thermistor acted as the four bridge legs. The feedback loop maintains the voltages of non-inverting and inverting inputs of the amplifier approximately equal by adjusting $V_2$. For example, when airspeed increases, the thermistor temperature decreases corresponding to an increase in thermistor resistance (NTC). This will cause the voltage difference between the non-inverting input and inverting input to increase; therefore, the output voltage from the amplifier increases, which through transistor increases $V_2$. As $V_2$ increases, the current passing through $R_t$ increases as well. The temperature of $R_t$ will increase, compensating for the temperature drop caused by increased airspeed; thus, maintaining thermistor temperature constant.

In addition, a NTC thermistor (nominal 10 kΩ at 25°C, NTCLE413-428, Vishay, Malvern, PA, USA) was used to measure ambient $t_{db}$ (not shown in figure 4). A divider circuit powered by the microcontroller supply voltage (assumed a constant +5.0 $V_{DC}$), featured a 10 kΩ resistor (±1% tolerance) in series with the $t_{db}$ thermistor to determine the $t_{db}$ thermistor resistance. The $t_{db}$

thermistor value was chosen to minimize the dissipated electrical power across the thermistor, as $t_{db}$ thermistor temperature can increase if the power is too high.

### 2.2.2 Analytical Analysis

Kirchhoff's current law was applied to the circuit (figure 1) to determine current flowing through the TA thermistor (equation 6).

$$I_t = \frac{(V_s - V_1)}{R_4} + \frac{(V_2 - V_1)}{R_6} \tag{6}$$

where

| | |
|---|---|
| $I_t$ | = current through the thermal anemometer thermistor (A) |
| $V_s$ | = supply voltage (+5.0 $V_{DC}$) |
| $V_1$ | = noninverting terminal voltage ($V_{DC}$) |
| $R_4$ | = resistance (10 kΩ) |
| $V_2$ | = emitter voltage ($V_{DC}$) |
| $R_6$ | = resistance (0.47 Ω) |

Further, resistance of the thermistor was found using Ohm's law (equation 7).

$$R_t = \frac{V_1}{I_t} \tag{7}$$

where

| | |
|---|---|
| $R_t$ | = thermistor resistance (Ω) |

Thermal anemometer thermistor resistance was used to find temperature, such that the temperature difference between the thermistor and $t_{db}$ could be determined. Likewise, power dissipated by the thermistor to the surrounding air (equation 8) was computed and used as an input to determine the heat dissipation factor (equation 1).

$$P = I_t\, V_1 \tag{8}$$

where

| | |
|---|---|
| $P$ | = power dissipated by the thermal anemometer (W) |

### 2.2.3 Software

A program developed in the integrated development environment for the microcontroller measured 60 analog voltages sequentially at $V_1$, $V_2$, and the ambient $t_{db}$ divider voltage ($V_{db}$),

approximately every 2 ms when prompted by a custom DAQ software (Matlab R2015b, The MathWorks Inc., Natick, MA, USA). Data were transmitted serially via a Universal Serial Bus (USB) cable to a computer with the DAQ software.

## 2.3 Calibration

### 2.3.1 Standard

Thermal anemometer calibration was performed with a custom wind tunnel standard constructed of an insulated (thermal resistance = 1.06 $m^2$ °C $W^{-1}$), 3.05 m long, 10.16 cm diameter schedule 40 PVC pipe, with a flow-straightener at the entrance of the pipe (figure 2). A cable grip to accommodate the airspeed sensor was inserted to a 1.27 cm diameter center bored hole, located 1.524 m from the inlet and 1.016 m from the outlet. This hole was at least ten pipe diameters from the closest upstream obstruction and at least five pipe diameters from the pipe exit to ensure fully-developed flow at the test position (ASHRAE, 2013). Located 90° from the test location, an additional cable grip was added to accommodate the $t_{db}$ thermistor. A 0.15 m diameter reducer also contained a flow-straighter and connected the pipe test section to a 0.61 m by 0.56 m by 0.89 m (H by W by L; interior) well-sealed, wood plenum. Both flow-straightening honeycomb sections were constructed with 5.08 cm long, 0.6 cm diameter plastic drinking straws. The inlet of the plenum contained a 5.08 cm diameter precision nozzle (Helander Metal Spinning Company, Lombard, IL, USA) with four throat static pressure taps. Static pressure was averaged and measured with a pressure transducer (sensitivity = 0.0804 $V_{DC}$ $Pa^{-1}$, Model 267, Setra Systems Inc., Boxborough, MA, USA). A 10.16 cm diameter schedule 40 PVC pipe connected to a variable speed inline fan mounted 1.3 m upstream of the nozzle inlet was used to control airflow through the test section. A variable speed device (AC-VXP/N:180V800E, Control Resources Inc., Littleton, MA, USA) transformed a 0 to 5 $V_{DC}$ input to control fan speed. Conditioned air supplied

to the test section was drawn via a 4.57 m long, 15.24 cm diameter insulated (thermal resistance = 1.41 $m^2$ °C $W^{-1}$) flexible duct from a large insulated plenum. An air handling unit (AA-5474, Parameter Generation and Control, Black Mountain, NC, USA) provided TE control of supply $t_{db}$ and supply RH (HMP-133Y, Vaisala, Helsinki, Finland) during calibration, which was modified from Ramirez, Hoff, Gao, & Harmon (2015).

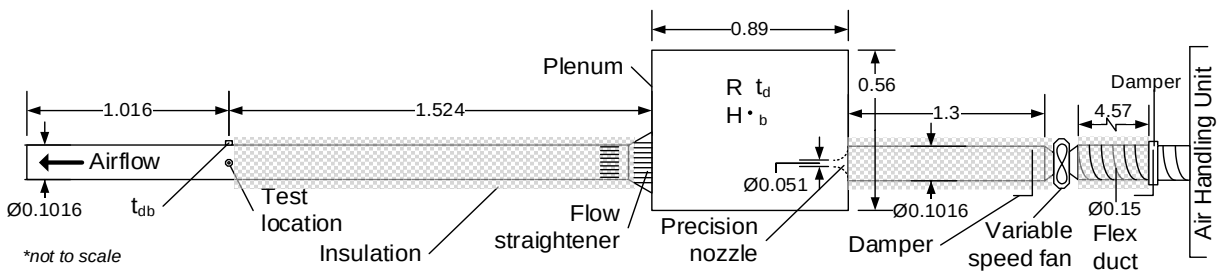


**Figure 2. Schematic of custom wind tunnel standard used to calibrate the thermal anemometer. Airspeed was controlled via a combination of varying damper positions and modifying fan speed. Dry-bulb temperature and RH was controlled by an air handling unit. All units in meters.**

Prior to TA calibration with the standard at the test location (figure 2), the reference air velocity at the test location was determined by regressing static pressure through the nozzle against air velocity measured by a reference hot-wire anemometer (sensitivity = 0.5 $V_{DC}$ (m $s^{-1}$)$^{-1}$, Model 8455, TSI Inc., Shoreview, MN, USA). The hot-wire anemometer was secured at the center of the pipe with the cable grip and allowed 1.5 min of stabilization time prior to initiating data collection. Twelve samples of data were recorded for one second, with 60 measurements per sample, from both the hot-wire anemometer and differential pressure transducer with the 14-bit ADC of a multifunction DAQ device (Model USB 1408FS, Measurement Computing Corp., Norton, MA, USA) at a set airflow. Airflows were randomly selected from ~0 to 6 m $s^{-1}$.

### 2.3.2 Data Acquisition and Procedure

The DAQ software controlled inline fan speed via the digital to analog converter (DAC) on

the multifunction DAQ device, and recorded analog outputs from the: differential pressure transducer, supply $t_{db}$, and supply RH via the multifunction DAQ device. In addition, the software transmitted the serial command to the microprocessor to initiate TA data collection.

The thermal anemometer was secured in the center pipe at the test location (figure 2) following the same procedure as the reference hot-wire anemometer, and the $t_{db}$ thermistor was secured in the other cable grip (figure 2). A total of 12 different airflows, corresponding to airspeeds from ~0 to 6 m $s^{-1}$ were conducted in random order. In addition, supply $t_{db}$ and RH were held constant during calibration and recorded with the multifunction DAQ device. At each airflow, six nominal dry-bulb temperatures (range) were tested: 18.0°C (16.5°C ≤ $t_{db}$ < 20.0°C), 21.5°C (20.0°C ≤ $t_{db}$ < 23.0°C), 24.5°C (23.0°C ≤ $t_{db}$ < 26.0°C), 27.0°C (26.0°C ≤ $t_{db}$ < 28.0°C), 29.5°C (28.0°C ≤ $t_{db}$ < 32.0°C), and 33.0°C (32.0°C ≤ $t_{db}$ < 35.0°C). Actual $t_{db}$ ranged for given a nominal $t_{db}$, for each airflow, due to heat losses downstream of the air handling unit. Calibration began 2 min after setting the airflow to allow the TA to stabilize in the flow field. The multifunction DAQ device was sampled for 1 s, collecting a total of 60 measurements, followed by TA data collection from the microprocessor. Data from the multifunction DAQ device and the microprocessor were recorded 12 times at each airflow, at randomly selected intervals (as generated by the DAQ software) ranging from 1 to 6 s to decouple any dependence on the prior measurements. Data were analyzed using Matlab (2015).

## 2.4 Time Constant

The time constant of the TA was determined by measuring the response to a step change from 0 to ~5.0 m $s^{-1}$ (equation 9) and from ~5.0 to 0 m $s^{-1}$ (equation 10). At the initial condition, measurements from the TA were made for 90 s to allow the system to stabilize followed by the step change, and monitored for an additional 45 s. This procedure was repeated six times each for

the step-up and step-down experiments. A nonlinear least squares regression (*Matlab*, 2015) of airspeed versus elapsed time was performed to determine the time constant (τ, ~63%) for introducing the TA to high and low flow fields. The time constants served as a metric to determine the time to reach steady-state. The time to reach steady-state was estimated by 3τ (~95% of the steady-state value), assuming first-order system behavior (equations 9 and 10).

$$u(t) = u_0 + \Delta u\left(1 - e^{\frac{-t+t_0}{\tau}}\right) \tag{9}$$

$$u(t) = u_0 + \Delta u\left(e^{\frac{-t+t_0}{\tau}}\right) \tag{10}$$

where

| | |
|---|---|
| $u(t)$ | = airspeed as a function of time (m s$^{-1}$) |
| $u_0$ | = initial $u$ at time $t_0$ (m s$^{-1}$) |
| $\Delta u$ | = difference between $u_0$ and $u$ at steady-state (m s$^{-1}$) |
| $t$ | = time (s) |
| $t_0$ | = initial time (s) |
| $\tau$ | = time constant (s$^{-1}$) |

## 2.5 Statistical Analysis

The standard uncertainty (denoted by Δ) associated with a measurement is a statistically based approximation of measurement error obtained from propagation of key measurement uncertainty sources (JCGM, 2008; Taylor & Kuyatt, 1994). A zeroth-order uncertainty budget, including Type A (the best available estimate of the expected value of a quantity that varies randomly) and Type B (not obtained from repeated observation, rather based on all available information) evaluations was performed for each sensor and essential hardware to determine the combined standard sensor uncertainty via summation of quadrature. Combined standard sensor uncertainties obtained from the zeroth-order analyses were then inputs that propagated through the analytical solutions (e.g., equations 6, 7, and 8). A truncated first-order Taylor series approximation, assuming independent measurements, was used to determine combined standard uncertainty associated with propagation of measurement error. Sensitivity coefficients (denoted by partial derivatives) were represented

for each input parameter and quantified how the combined standard uncertainty changed with variations of its inputs (JCGM, 2008). A sensitivity analysis was performed to determine the key contributions of input parameters on the combined standard uncertainty associated with $t_t$, $t_{db}$, $\delta$, reference air velocity, and ultimately, the predicted airspeed obtained by the TA.

### 2.5.1 Sensor Module

The TA thermistor temperature was found by regressing the Hoge-2 equation (Hoge, 1988) through data (resistance reported at 1°C increments) provided by the TA thermistor manufacturer for the anticipated operation range of 50°C to 150°C (equation 11). After calculation of TA thermistor temperature equation 11, the TA thermistor temperature was converted from Kelvin to Celsius for subsequent use.

$$T_t^{-1} = a_1 + a_2 \ln R_t + a_3 \ln R_t^2 + a_4 \ln R_t^3 \tag{11}$$

where

$T_t$ = thermal anemometer thermistor temperature (K)
$R_t$ = thermistor resistance (Ω)
$a_1$-$a_4$ = coefficients

Key parameters required to compute the $R_t$ included two analog voltage measurements ($V_1$ and $V_2$) and two bridge resistor values ($R_4$ and $R_6$). The standard uncertainty associated with these inputs was evaluated and propagated through the nonlinear regression equation (equation 11) to determine the combined standard uncertainty with $T_t$. A zeroth-order uncertainty budget, including sources from Type A and Type B evaluations was created for analog voltage measurement by the TA microcontroller (table 1) for subsequent use to determine $T_t$ and $\delta$.

**Table 1. Uncertainty budget for analog voltage measurement by microcontroller analog to digital converter.**

| Source | Value ($V_{DC}$) | Probability distribution | Divisor | Standard uncertainty ($V_{DC}$) |
|---|---|---|---|---|
| Repeatability[a] | 0.0012 | Normal | 1 | 0.0012 |
| Quantization error[b] | 0.0024 | Rectangular | √3 | 0.0014 |
| Display resolution[c] | 5.0E-05 | Rectangular | √3 | 2.89E-05 |
| Combined sensor standard uncertainty, $\Delta V$ | | | | 0.0019 |

[a] Largest SE of 30 measurements as found from five constant voltage tests (1.000, 2.501, 3.001, 3.501, and 4.001 V)
[b] ±0.5 ATmega32U4 10-bit ADC resolution = 0.005 V $BL^{-1}$
[c] ±0.5 smallest display value = 0.0001

Chauvenet's criterion with a maximum allowable deviation of less than 2.618 (n = 60) was applied to the analog voltage measurements in the 60 measurement sample sent from the microcontroller. Data that satisfied the criterion was averaged, such that there was twelve means that represented a given air velocity. Those twelve means were averaged again to represent one value for a given airspeed. The standard error of the mean was calculated from this result (n = 12).

The standard uncertainty associated with a mean analog voltage (equation 12) was determined by summing the uncertainty propagated through the computation of the arithmetic mean with the SE of the mean in quadrature.

$$\Delta\bar{V}_j^{\,2} = \frac{\Delta V_j^{\,2}}{n} + SE^2 \tag{12}$$

where

$j$ = analog voltage measurement location ($V_1$, $V_2$, $t_{db}$ divider, and dP transducer)
$\Delta\bar{V}_j$ = mean analog voltage combined standard uncertainty ($V_{DC}$)
$\Delta V_j$ = analog voltage combined standard uncertainty ($V_{DC}$; table 1)
$SE$ = standard error of the mean measured analog voltages ($V_{DC}$)

The standard uncertainty associated with calculating $R_t$ (equation 13) was determined from the propagation of mean analog voltage standard uncertainty (equation 12) and the standard uncertainty of the resistors in the bridge circuit (figure 1). A rectangular probability distribution (JCGM, 2008) was assigned to the manufacturer's non-traceable tolerance for the bridge resistors.

$$\Delta R_t^{\,2} = \left(\frac{\partial R_t}{\partial \bar{V}_1}\Delta\bar{V}_1\right)^2 + \left(\frac{\partial R_t}{\partial \bar{V}_2}\Delta\bar{V}_2\right)^2 + \left(\frac{\partial R_t}{\partial R_4}\Delta R_4\right)^2 + \left(\frac{\partial R_t}{\partial R_6}\Delta R_6\right)^2 \tag{13}$$

where

$\Delta R_t$ = thermal anemometer thermistor resistance combined standard uncertainty (Ω)
$\Delta R_4$ = resistor standard uncertainty (± 1%; Ω; rectangular distribution)

$\Delta R_6$ = resistor standard uncertainty (± 1%; Ω; rectangular distribution)

The standard uncertainty associated with the nonlinear regression (equation 11) to predict $T_t$ was determined by computing the Root-Mean-Square Error (*RMSE*; equation 14).

$$RMSE = \left(\frac{1}{n}\sum_{i=1}^{n}(y_i - \hat{y}_i)^2\right)^{1/2} \tag{14}$$

where

$n$ = number of data
*RMSE* = root mean square error (dependent variable units)
$y_i$ = dependent variable
$\hat{y}_i$ = predicted value from the regression

The combined standard uncertainty associated with thermistor temperature (equation 15) was determined from $\Delta R_t$ (equation 13), the manufacturer's accuracy, and the nonlinear regression statistics (equation 14).

$$\Delta {t_t}^2 = \left(\frac{\partial t_t}{\partial R_t}\Delta R_t\right)^2 + ACC^2 + RMSE^2 \tag{15}$$

where

$\Delta t_t$ = thermal anemometer thermistor temperature combined standard uncertainty (°C)
*ACC* = manufacturer's accuracy (± 2.0°C; rectangular distribution)
*RMSE* = root mean square error from nonlinear regression (°C; equation 14)

The temperature of the $t_{db}$ thermistor was found by regressing the Hoge-2 equation (Hoge, 1988) through data (resistance reported at 5°C increments) provided by the manufacturer for the anticipated operation range of -25°C to 45°C (equation 16). After calculation of $t_{db}$ thermistor temperature by equation 16, the $t_{db}$ thermistor temperature was converted from Kelvin to Celsius for subsequent use.

$${T_{db}}^{-1} = b_1 + b_2 \ln R_{db} + b_3 \ln {R_{db}}^2 + b_4 \ln {R_{db}}^3 \tag{16}$$

where

$T_{db}$ = $t_{db}$ thermistor temperature (K)
$R_{db}$ = thermistor resistance (Ω)
$b_1$-$b_4$ = coefficients

The uncertainty associated with $t_{db}$ thermistor temperature (equation 17) was determined from

the propagation of analog voltage uncertainty (table 1) and divider resistor uncertainty through the analytical solution to the resistor divider circuit using Ohm's law. A rectangular probability distribution was assigned to the manufacturer's non-traceable tolerance for the divider resistor (10 kΩ). Further, the nonlinear regression (equation 16) statistics also contributed. The microcontroller operating voltage (not measured) was assumed to be constant (+5.0 $V_{DC}$) and have negligible standard uncertainty; thus, excluded from the analysis.

$$\Delta t_{db}{}^2 = \left(\frac{\partial t_{db}}{\partial R_a}\Delta R_a\right)^2 + \left(\frac{\partial t_{db}}{\partial \bar{V}_{db}}\Delta \bar{V}_{db}\right)^2 + ACC^2 + RMSE^2 \tag{17}$$

where

| | |
|---|---|
| $\Delta t_{db}$ | = dry-bulb temperature combined standard uncertainty (°C) |
| $\Delta R_a$ | = 10 kΩ resistor in divider circuit (± 1%; Ω; rectangular distribution) |
| *ACC* | = manufacturer's accuracy (± 0.5°C; rectangular distribution) |
| *RMSE* | = root mean square error from nonlinear regression (°C) |

### 2.5.2 Standard

A relationship between the precision nozzle differential static pressure and air velocity measured by the reference hot-wire anemometer at the test location (figure 2) was developed using a piecewise higher-order polynomial regression (equation 18). One discontinuity was selected at the point where the *RMSE* for both functions was minimized; hence, two independent regressions of equation 18 were obtained. Both regressions were then used to determine the reference air velocity based on the precision nozzle differential static pressure during TA calibration.

$$u_{ref} = c_1 dP^3 + c_2 dP^2 + c_3 dP + c_4 \tag{18}$$

where

| | |
|---|---|
| $u_{ref}$ | = reference airspeed at center of pipe (m $s^{-1}$) |
| $dP$ | = precision nozzle differential static pressure (Pa) |
| $c_1$-$c_4$ | = coefficients |

A zeroth-order uncertainty budget was created for the differential static pressure transducer (table 2) and for the reference hot-wire anemometer (table 3). Results of this uncertainty budget, along with the nonlinear regression statistics, were combined and subsequently used as inputs to

determine the overall uncertainty associated with the reference air velocity at TA calibration.

**Table 2. Uncertainty budget for differential static pressure transducer.**

| Source | Value (Pa) | Probability distribution | Divisor | Standard uncertainty (Pa) |
|---|---|---|---|---|
| Accuracy RSS[a] | 1.244 | Rectangular | √3 | 0.7182 |
| Long term stability | 0.1244 | Rectangular | √3 | 0.0718 |
| Quantization error[b] | 0.0076 | Rectangular | √3 | 0.0044 |
| Combined standard sensor uncertainty, $\Delta dP$ | | | | 0.7218 |

[a] Root Sum Square (at constant $t_{db}$), ±1.0 % full scale (0 – 124.4 Pa)
[b] ±0.5 sensor resolution = (14-bit ADC resolution, 20 $V_{DC}$ reference range = 3.05E-4 V $BL^{-1}$) (sensor sensitivity)$^{-1}$

**Table 3. Uncertainty budget for hot-wire anemometer; where, $u_{meas}$ was evaluated at an arbitrary 0.23 and 5.55 m $s^{-1}$ to show the standard uncertainty range for the sensor.**

| Source | Value (m $s^{-1}$) | Probability distribution | Divisor | Standard uncertainty (m $s^{-1}$) |
|---|---|---|---|---|
| Quantization error[a] | 6.104E-4 | Rectangular | √3 | 3.5239E-4 |
| Accuracy[b] | $0.02(u_{meas}) + 0.05$ | Rectangular | √3 | 0.0316 – 0.0930 |
| Repeatability[c] | $0.01(u_{meas})$ | Normal | 1 | 0.0023 – 0.0556 |
| Resolution[d] | 0.007 | Rectangular | √3 | 0.0040 |
| Combined standard sensor uncertainty, $\Delta u_{ref}$ | | | | 0.0319 – 0.1084 |

[a] ±0.5 sensor resolution = (14-bit ADC resolution, 10 $V_{DC}$ reference range = 0.0012 V $BL^{-1}$) (sensor sensitivity)$^{-1}$
[b] ±2% of reading plus 0.5% of full scale range (0 – 10 m $s^{-1}$) = 0.05 m $s^{-1}$
[c] < ±1.0% of reading (based on one minute average standard deviation)
[d] 0.07% of selected full scale (0 – 10 m $s^{-1}$)

Propagation of uncertainty obtained from the zeroth-order uncertainty budgets (tables 2 and 3) through the reference nonlinear regression (equation 18), combined with the *RMSE*, yielded the combined standard uncertainty associated with the reference air velocity at TA calibration (equation 19).

$$\Delta u'_{ref}{}^{2} = \left(\frac{\partial u'_{ref}}{\partial dP}\Delta dP\right)^{2} + RMSE^{2} + \left(\Delta u_{ref}\right)^{2} \tag{19}$$

where

$\Delta u'_{ref}$ = reference airspeed combined standard uncertainty (m $s^{-1}$)

### 2.5.3 Heat Dissipation Factor

The standard uncertainty associated with calculation of $\delta$ (equation 20) was determined from the propagation of uncertainty in the input parameters.

$$\Delta\delta^2 = \left(\frac{\partial\delta}{\partial\bar{V}_1}\Delta\bar{V}_1\right)^2 + \left(\frac{\partial\delta}{\partial\bar{V}_2}\Delta\bar{V}_2\right)^2 + \left(\frac{\partial\delta}{\partial R_4}\Delta R_4\right)^2 + \left(\frac{\partial\delta}{\partial R_6}\Delta R_6\right)^2 + \left(\frac{\partial\delta}{\partial t_t}\Delta t_t\right)^2 + \left(\frac{\partial\delta}{\partial t_{db}}\Delta t_{db}\right)^2 \quad (20)$$

where

$\Delta\delta$ = heat dissipation factor combined standard uncertainty (W °C$^{-1}$)

### 2.5.4 Calibration

A piecewise higher-order polynomial regression was obtained from the calibration data at airspeeds from ~0.0 to ~5.5 m s$^{-1}$, over a nominal $t_{db}$ range (18°C to 33°C) to determine the $t_{db}$ compensated airspeed (equation 21) using the relationship described in equation 5 and proposed by Hultmark & Smits (2010). One discontinuity in the calibration data was selected at the point where the *RMSE* for both functions was minimized; hence, two independent regressions of equation 21 were obtained.

$$\frac{u'}{\nu} = d_1\left(\frac{\delta}{k}\right)^3 + d_2\left(\frac{\delta}{k}\right)^2 + d_3\frac{\delta}{k} + d_4 \quad (21)$$

where

$u'$ = predicted airspeed with $t_{db}$ compensation (m s$^{-1}$)

$d_1$ - $d_4$ = coefficients

Predicted airspeed combined standard uncertainty (equation 22) was determined by propagation of parameter uncertainty in equation 5 and the addition of the nonlinear regression statistics. Air properties (i.e., thermal conductivity, absolute viscosity, and density) were assumed to have negligible uncertainty.

$$\Delta u'^2 = \left(\frac{\partial u'}{\partial\delta}\Delta\delta\right)^2 + \Delta u'_{ref}{}^2 + RMSE^2 \quad (22)$$

where

$\Delta u'$ = predicted airspeed combined standard uncertainty (m s$^{-1}$)

# 3 Results and Discussion

## 3.1 Sensor Module

The final cost of the Thermal Anemometer (TA) system was approximately $35 USD (including circuit components and microcontroller, but excluding labor). Cost of commercially

available low velocity anemometers can be substantially more and do not include stated standard uncertainty. At 22°C, ~0.103 A (325 mW) of current at 5 $V_{DC}$ was supplied to the TA system in still air and ~0.139 A (695 mW) in a ~5.5m $s^{-1}$ flow field.

Coefficients for the nonlinear regression of the Hoge-2 equation (equation 11) to determine TA thermistor temperature ($t_t$) were $a_1$ = 1.638E-3, $a_2$ = 2.77E-4, $a_3$ = -1.718E-6, and $a_4$ = 3.3536E-7. The coefficient of determination ($R^2$) = 1 and RMSE = 0.0064°C.

Average (±standard deviation) $t_t$ during calibration was 103.7°C (±0.29°C) with an associated combined standard uncertainty ($\Delta t_t$) ranging from 0.8°C to 1.9°C (figure 3). It is important during TA operation that $t_t$ is constant and consistent at different airspeeds and $t_{db}$ to ensure repeatable results. This critical low distribution $t_t$ is also observed in figure 3. There is no apparent trend between $t_{db}$ and $\Delta t_t$ (figure 3), but it is important $\Delta t_t$ is minimized to avoid propagating the uncertainty through the subsequent equations. The sensitivity analysis showed on average that analog voltage ($\Delta V_1$ and $\Delta V_2$) measurement uncertainty combined for a ~95.9% (±1.5% each) contribution to $\Delta t_t$, while the bridge resistor ($R_4$ and $R_6$) uncertainties contributed on average <<1% and 4.1% (±1.5%), respectively. The *RMSE* from the Hoge-2 regression contributed much less 1%.

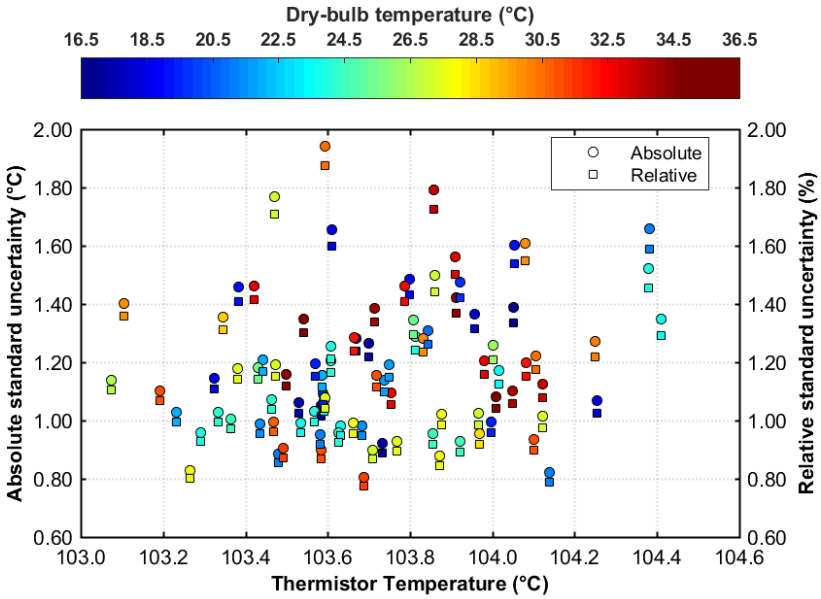


**Figure 3. Absolute and relative combined standard uncertainty associated with thermistor temperature measurement during thermal anemometer calibration.**

Coefficients for the nonlinear regression of the Hoge-2 equation (equation 16) to determine dry-bulb thermistor temperature ($t_{db}$) were $b_1$ = 7864E-4, $b_2$ = 2821E-4, $b_3$ = -3.01E-6, and $b_4$ = 2.877E-7. The $R^2$ = 1 and RMSE = 6.971E-4°C.

Combined standard uncertainty associated with $t_{db}$ ($\Delta t_{db}$) measurement during calibration (16.5°C $\leq$ $t_{db}$ $\leq$ 35.5°C) ranged from 0.32°C (at 16.8°C) to 0.33°C (at 33.3°C; figure 4), corresponding to 1.93% to 0.95%, respectively, of the actual measurement. The sensitivity analysis showed the manufacturer's accuracy to contribute the greatest to $\Delta t_{db}$ (~79%), followed by the voltage divider resistor tolerance (~21%) and lastly, the analog voltage measurement (<<1%). Since, manufacturer's accuracy dominates the relative contribution to $\Delta t_{db}$, the steady absolute $\Delta t_{db}$ is reasonable (figure 4).

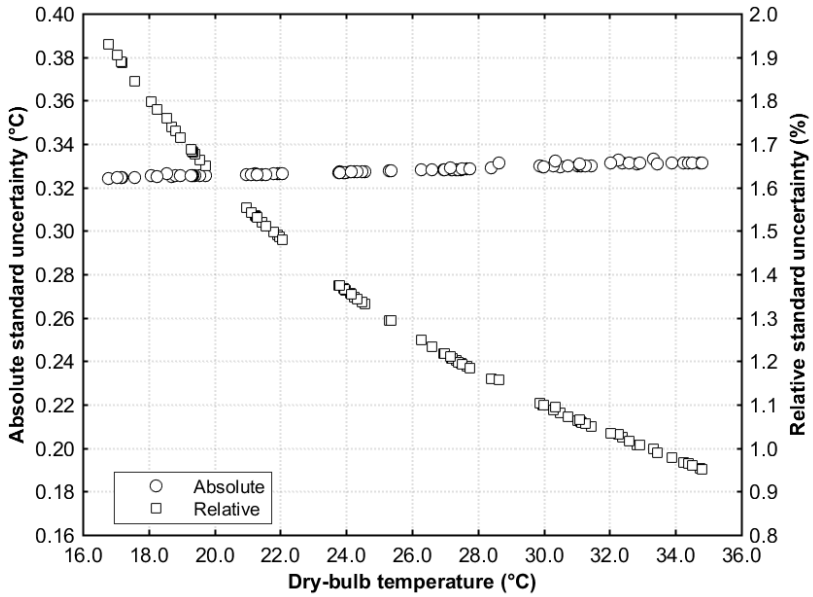


**Figure 4. Absolute and relative combined standard uncertainty associated with dry-bulb temperature measurement during thermal anemometer calibration.**

## 3.2 Standard

The piecewise nonlinear regression for the reference velocity measured at the test location and the differential static pressure across the precision nozzle (figure 5; equation 18) yielded two sets of coefficients: (1) $c_1$ = 0.0004627, $c_2$ = -0.01428, $c_3$ = 0.2579, and $c_4$ = -0.5563 for airspeeds less than 1.4 m $s^{-1}$ ($R^2$ = 0.9965; RMSE = 0.0282 m $s^{-1}$), and (2) $c_1$ = 2.97e-06, $c_2$ = -0.0009404, $c_3$ = 0.139, and $c_4$ = -0.3354 ($R^2$ = 0.9944; RMSE = 0.1095 m $s^{-1}$) for airspeeds greater than 1.4 m $s^{-1}$. The discontinuity at 1.4 m $s^{-1}$ (figure 5) was chosen to have the smallest *RMSE* for both high and low velocities. If a continuous nonlinear regression was fit through that data, the *RMSE* would be 0.0937 m $s^{-1}$, compared to a *RMSE* of 0.0282 m $s^{-1}$, obtained from the regression through data less than 1.4 m $s^{-1}$. At a nominal 0.5 m $s^{-1}$, the continuous regression *RMSE*, on a relative basis, would be 18.7% of the nominal airspeed, while the piecewise regression was only 5.6%. Turbulence intensity at the pipe core (location of airspeed sensors) ranged from 4.3% to 5.9% for all flows.

The maximum differential static pressure standard deviation was 2.27 Pa at 0.09 m s$^{-1}$, suggesting the reference was stable within the margin of quantified doubt at a constant air velocity.

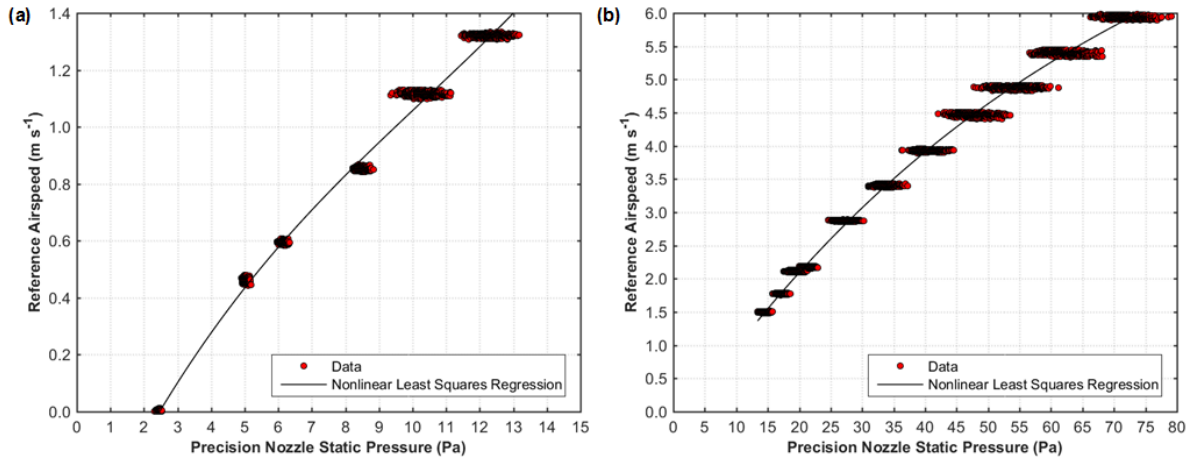


**Figure 5. Piecewise nonlinear regressions for low airspeed (a) and high airspeeds (b) used to determine the reference airspeed at the test location based on precision nozzle differential static pressure obtained from the standard.**

The combined standard uncertainty of the reference velocity ($\Delta u'_{ref}$) used to calibrate the TA ranged from 0.05 to 0.16 m s$^{-1}$ over a ~0.0 to 5.9 m s$^{-1}$ range (figure 6). Relative $\Delta u'_{ref}$ was greater at low velocities due to the reference's reading scale plus 0.05 percent full scale accuracy (table 3; figure 7). At less than 1.4 m s$^{-1}$, relative $\Delta u'_{ref}$ (figure 6) ranged from 4.4% (0.05 m s$^{-1}$ at 1.3 m s$^{-1}$) to 13.0% (0.06 m s$^{-1}$ at 0.4 m s$^{-1}$). When greater than 1.4 m s$^{-1}$ relative $\Delta u'_{ref}$ ranged from 2.7% (0.16 m s$^{-1}$ at 5.9 m s$^{-1}$) to 8.3% (0.12 m s$^{-1}$ at 1.5 m s$^{-1}$). Separation of the regressions was critical to reducing uncertainty at low velocities. Since, the *RMSE* is constant over the entire regression, this causes large relative uncertainties at low velocities. This can be improved by using two separate nonlinear regressions to reduce the overall standard uncertainty at low velocities. While it is uncommon to possess uncertainty in the calibration standard or reference, this experimental setup does have measurement error for its standard values (i.e., velocity and differential pressure) and must be accounted in the overall uncertainty associated TA airspeed measurement and

prediction.

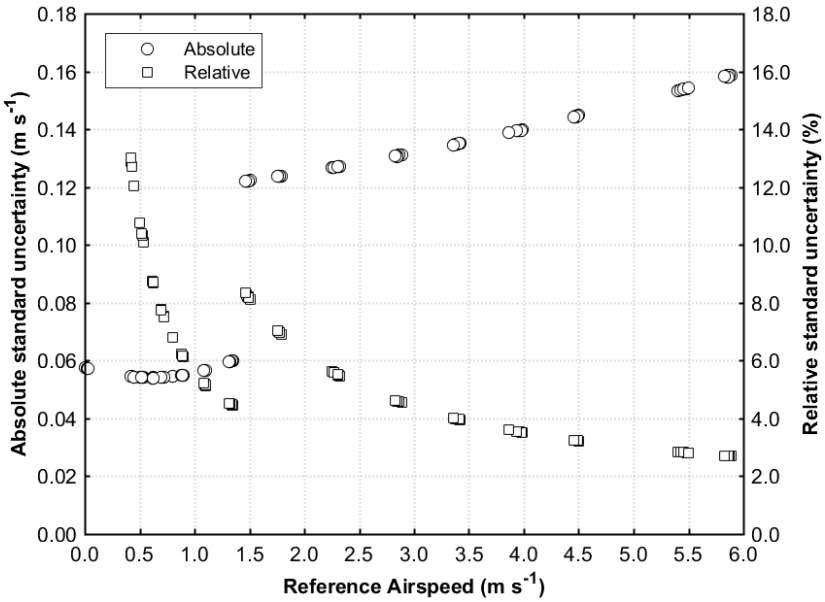


**Figure 6. Absolute and relative combined standard uncertainties for the reference airspeed at the center of the pipe used to determine the overall combined standard uncertainty associated with measured airspeed. The discontinuity at 1.4 m s$^{-1}$ is due to the fact that two individual regressions were applied; thus, separating influence of the *RMSE* on the reference combined standard uncertainty.**

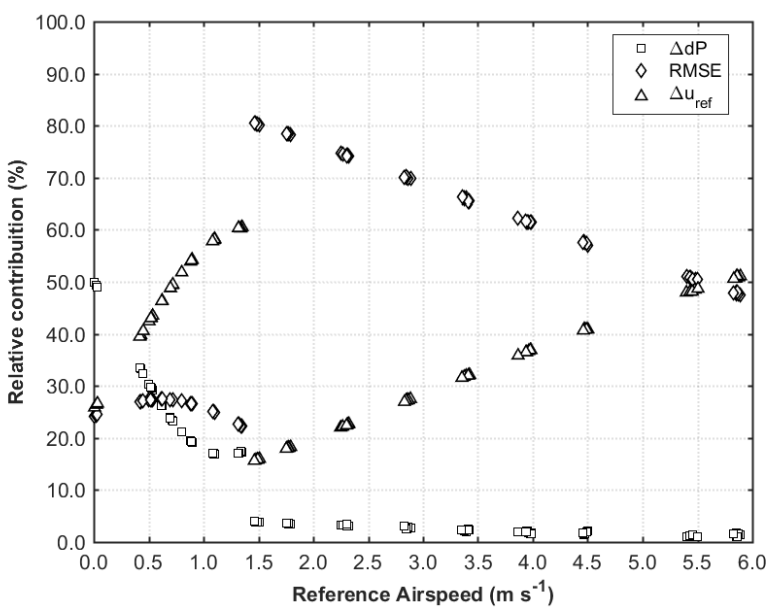


**Figure 7. Sensitivity analysis for reference velocity combined standard uncertainty. The discontinuity at 1.4 m s$^{-1}$ is due to the fact that two individual regressions were applied; thus, separating influence of the *RMSE* on the reference combined standard uncertainty**

### 3.3 Calibration

At six nominal $t_{db}$ (range), 18.0°C (16.5°C ≤ $t_{db}$ < 20.0°C), 21.5°C (20.0°C ≤ $t_{db}$ < 23.0°C), 24.5°C (23.0°C ≤ $t_{db}$ < 26.0°C), 27.0°C (26.0°C ≤ $t_{db}$ < 28.0°C), 29.5°C (28.0°C ≤ $t_{db}$ < 32.0°C), and 33.0°C (32.0°C ≤ $t_{db}$ < 35.0°C), results showed a physical relationship between the heat dissipation factor ($\delta$) and $t_{db}$ (figure 8), which is indicative of previous findings and heat transfer theory (Abdel-Rahman, Tropea, Slawson, & Strong, 1987; Bowers, Willits, & Bowen, 1988; Hultmark & Smits, 2010). Relative humidity was maintained at an average 49.9% ±3.3% through calibration. Heat dissipation factors ranged from approximately 1.5 (0 m $s^{-1}$; all nominal $t_{db}$) to 4.3 mW °$C^{-1}$ (5.9 m $s^{-1}$; 18°C nominal $t_{db}$). As air velocity decreased, convective losses also decreased; thus, a smaller relative difference between $\delta$ across $t_{db}$. At a given velocity, $\delta$ was expected to be lower for warmer $t_{db}$ based on heat transfer theory, increasing in magnitude to the coldest $t_{db}$. This trend appears to be evident in the collected data, for example, clearly shown at a nominal 4 and 3.5 m $s^{-1}$ (figure 8). In general, at a given airspeed $\delta$ was lower for warmer $t_{db}$ compared with colder $t_{db}$. Uncertainties in the measurement system and calibration reference most likely contributed to inconsistencies among $\delta$ at a given velocity, resulting in some measured $\delta$ not exactly adhering to heat transfer theory.

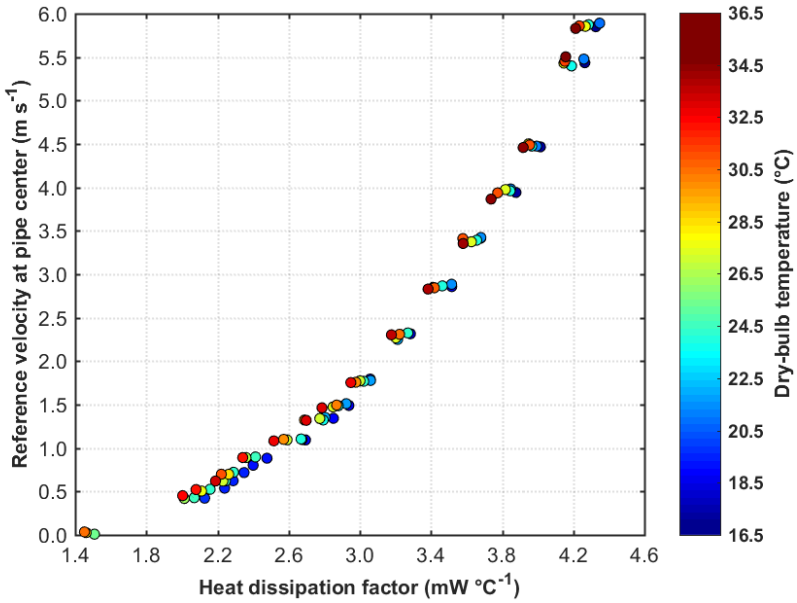


**Figure 8. Thermal anemometer calibration data colored by actual dry-bulb temperature.**

Heat dissipation factor combined standard uncertainty ($\Delta\delta$; figure 9) ranged from about 0.06 to 0.08 at 0 m s$^{-1}$ (any nominal $t_{db}$ tested) to 0.17 mW °C$^{-1}$ at 5.8 m s$^{-1}$ (nominal 33°C). No apparent pattern between airspeed and $t_{db}$ with $\Delta\delta$ was evident. Relative $\Delta\delta$ ranged from 2.4% at 5.5 m s$^{-1}$ (nominal 21°C) to 5.8% at 0 m s$^{-1}$ (nominal 31°C; figure 9). For a given reference velocity, the maximum absolute difference between $\delta$ at the warmest and colder $t_{db}$ was approximately 0.1 mW °C$^{-1}$. Since it can be assumed that the possible estimated values of the parameters contributing to the calculation of $\delta$ are approximately normally distributed with approximate standard deviation represented by $\Delta\delta$, the unknown value of $\delta$ is believed to lie in the interval defined by combined standard uncertainty with a level of confidence of approximately 63% (Taylor & Kuyatt, 1994). While $\delta$ for any nominal $t_{db}$ range is not statistically different, a physical relation still exists; hence, $t_{db}$ compensation is still required.

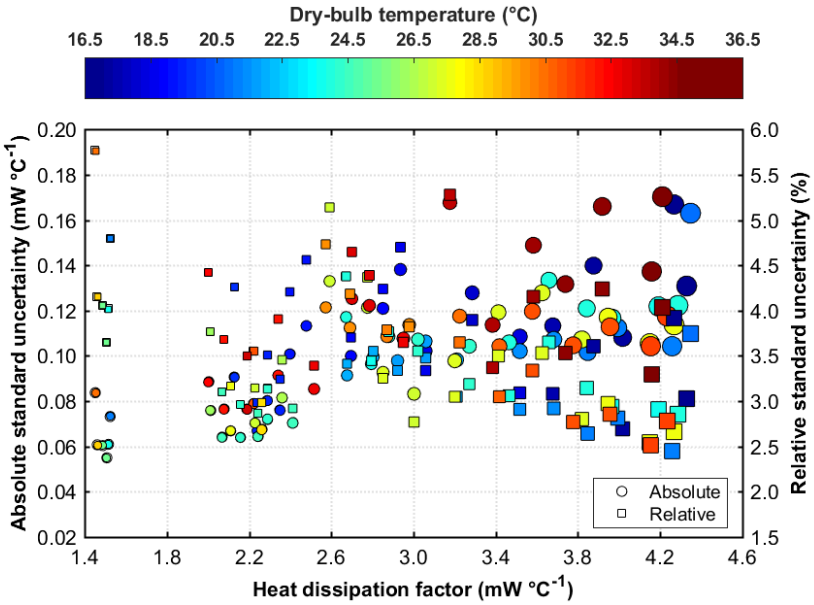


**Figure 9. Absolute and relative combined standard uncertainty associated with heat dissipation factor calculation during thermal anemometer calibration. Marker area size correlates to reference velocity during calibration.**

The sensitivity analysis showed analog voltage measurement were the greatest contributors (figure 10) to $\Delta\delta$, with a combined average of 74.9% (2.5%). This result was most likely attributed to the 10-bit ADC resolution of the microcontroller. Given the number of measurements and the importance of $V_1$, $V_2$, and $V_{db}$, in determining $\delta$, the ADC resolution was the limiting factor in the TA system. However, the low cost, ease of use, and wide functionality of the microcontroller makes it suitable for multi-point measurement applications. An increase in the ADC resolution could decrease $\Delta\delta$ and ultimately improve the TA. Other parameters on average, such as, bridge resistors ($R_4$ and $R_6$) uncertainty (2.9%), $\Delta t_t$ (20.6%), and $\Delta t_{db}$ (1.6%) contributed to $\Delta\delta$.

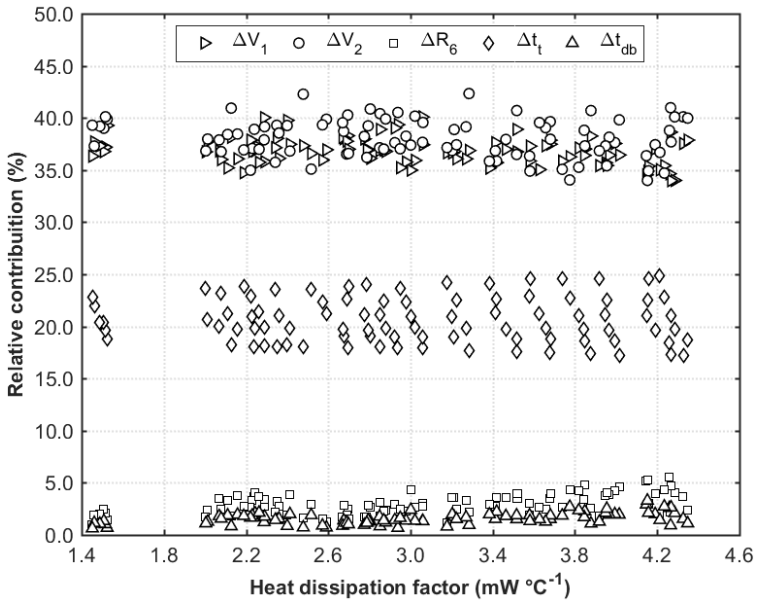


**Figure 10. Sensitivity analysis for combined standard uncertainty associated with heat dissipation factor calculation during thermal anemometer calibration. Bridge resistor $R_4$ was omitted for clarity and its low contribution to heat dissipation factor uncertainty.**

Coefficients for the fourth-order polynomial dry-bulb temperature compensation regression (equation 21; figure 11) at velocities <2 m $s^{-1}$ were $d_1$ = 1.282E07, $d_2$ = 1.081E07, $d_3$ = -4.099E05, $d_4$ = -9.219E03 ($R^2$ = 0.9842; RMSE = 0.0675 m $s^{-1}$), and at velocities ≥2 m $s^{-1}$ were $d_1$ = -1. 049E09, $d_2$ = 4.495E08, $d_3$ = -5.897E07, $d_4$ = 2.549E06 ($R^2$ = 0.9857; RMSE = 0.1462 m $s^{-1}$). The discontinuity at 2.0 m $s^{-1}$ (figure 5) was chosen to have the smallest *RMSE* for both high and low velocities. If a continuous nonlinear regression was fit through that data, the *RMSE* would be 0.1176 m $s^{-1}$, compared to the 0.0675 m $s^{-1}$ obtained for the regression through data less than 2 m $s^{-1}$. At a nominal 0.5 m $s^{-1}$, the continuous regression *RMSE*, on a relative basis, would be 23.5% of the nominal airspeed, while the piecewise regression was only 13.5%. The regression statistics for each curve demonstrates that the proposed correction technique by Hultmark and Smits (2010) accurately describes the influences of different $t_{db}$ on the calibration.

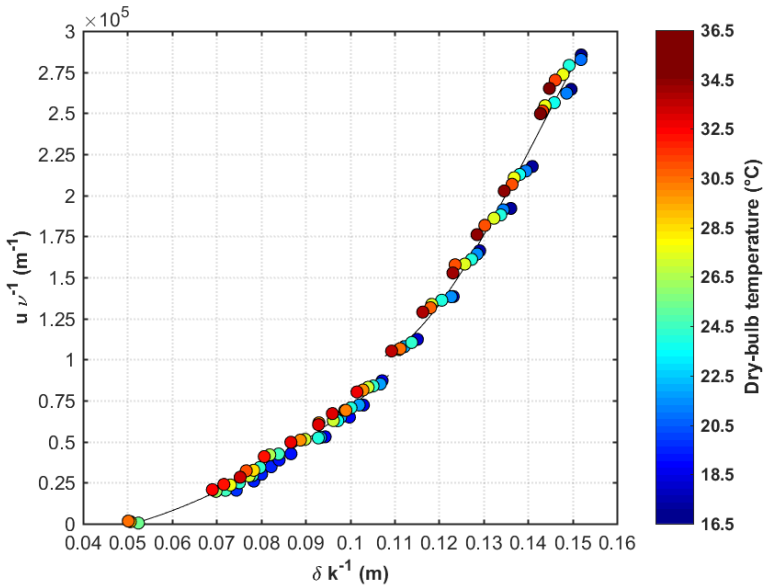


**Figure 11. Thermal anemometer calibration with $t_{db}$ compensation. Two unique fourth-order polynomial regressions were used to separate velocities <2 m s$^{-1}$ and ≥2 m s$^{-1}$ to reduce uncertainty at low velocities.**

The combined standard uncertainty associated with predicted airspeed ($\Delta u'$) ranged from 0.11 (at 0.46 m s$^{-1}$) to 0.71 m s$^{-1}$ (at 5.52 m s$^{-1}$; figure 12). At low velocities, there were small differences among $\Delta u'$, while at higher velocities, $\Delta u'$ varied much more as shown by the dispersion of circular markers in figure 12. This was most likely due to the turbulent velocities at the higher airspeeds. For this reason, two separate regression were used such that the larger *RMSE* at the higher velocities does not impact the $\Delta u'$ at the lower velocities. Relative $\Delta u'$ decreased as velocity increased, with a range from 7.85% (5.67 m s$^{-1}$) to 30.3% (0.40 m s$^{-1}$). Due to the propagation of measurement error through the uncertainty analysis, measured airspeeds are believed to lie in the interval defined by $\Delta u'$ with a level of confidence of approximately 63%. The sensitivity analysis (figure 13) showed for velocities <2 m s$^{-1}$, the relative contribution of $\Delta\delta$ to initially increase as velocity increased and then decrease as the discontinuity was approached. While *RMSE* and $\Delta u_{ref}$ were similar in magnitude and decreasing as velocity increased, the relative contribution of $\Delta u_{ref}$ began to increase as the discontinuity was approached. For velocities increasing beyond 2 m s$^{-1}$,

the *RMSE* and $\Delta u_{ref}$ had similar magnitude and trend (figure 13), while the relative contribution of $\Delta\delta$ increased. A decrease in the overall uncertainty associated with the reference and the microcontroller ADC, to reduce the uncertainty in $\delta$, may ultimately lead to a decrease in $\Delta u'$.

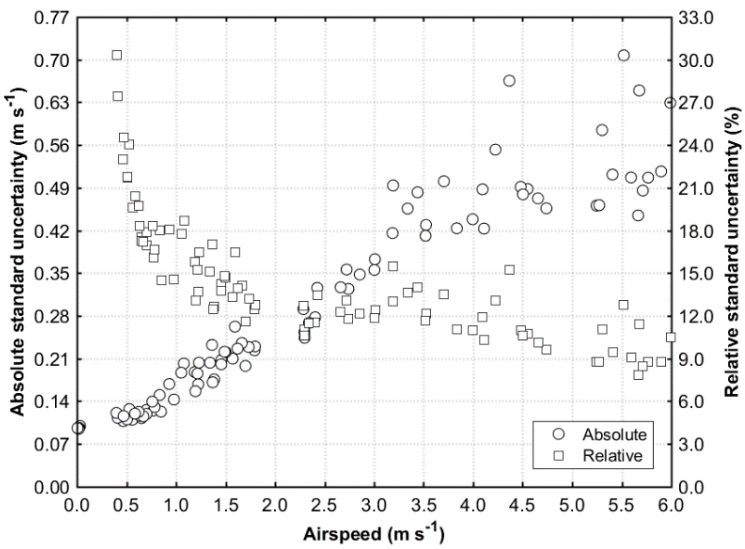


**Figure 12. Absolute and relative combined standard uncertainty associated with thermal anemometer predicted airspeed with $t_{db}$ compensation during calibration.**

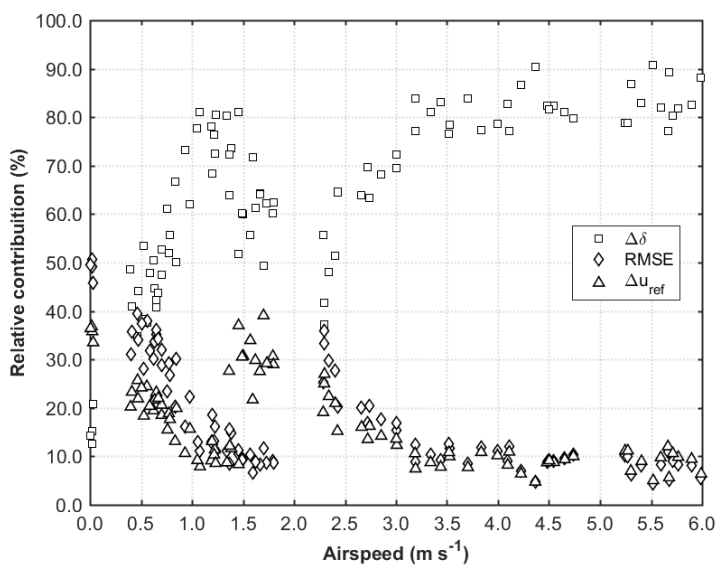


**Figure 13. Sensitivity analysis for combined standard uncertainty associated with thermal anemometer predicted airspeed during calibration.**

### 3.4 Time Constant

Average (±standard deviation) time to reach steady-state (3τ) was 3.14 ±0.31 s (step-up) and 2.15 ±0.20 s (step-down; table 4; figure 14). The $R^2$ were ~0.94 (step-up) and greater than 0.99 (step-down) for each regression. The *RMSE* provided an estimate of the overall uncertainty over the regression. The step-up caused the system to reach steady-state slower compared with the step-down, due to the behavior of the bridge circuit generating more power to maintain a constant temperature at the thermistor (figure 14). Time to reach steady-state was used to improve experimental and operational protocols. That is, the TA has limited applications in turbulent flows where airspeed may be changing faster than 3τ.

**Table 4. Nonlinear regression coefficients and statistics summary for time constant and time to reach steady-state for a step-up and step-down.**

| Step change (m $s^{-1}$) | τ ($s^{-1}$) | $R^2$ | RMSE (m $s^{-1}$) | Time to reach steady-state (s) |
|---|---|---|---|---|
| 0 to ~5 | 1.05 ±0.10 | ~0.94 | 0.19 ±0.01 | 3.14 ±0.31 |
| ~5 to 0 | 0.72 ±0.07 | >0.99 | 0.04 ±0.01 | 2.15 ±0.20 |

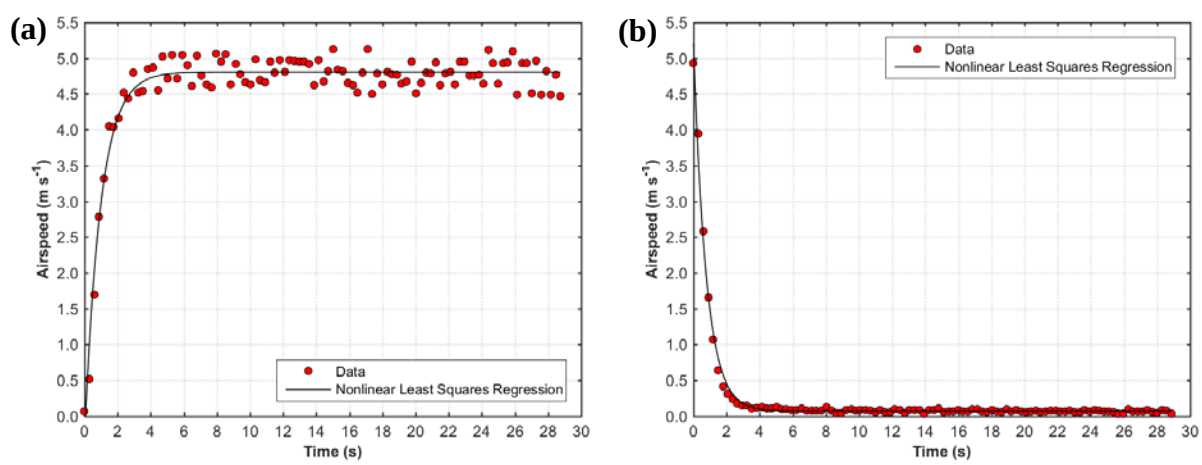


**Figure 14. Nonlinear regression and data to determine the time constant for step-up (a) and step-down (b).**

# 4 Conclusions

A constant temperature thermal anemometer with a measurement range between 0 and 6 m $s^{-1}$ with dry-bulb temperature compensation was designed, constructed, and calibrated with an

absolute standard uncertainty ranging from approximately 0.11 to 0.71 m $s^{-1}$ and a relative standard uncertainty ranging from approximately 7.85% to 30.3%. The low-cost (less than $35 USD excluding labor) and simple hardware, make this thermal anemometer well-suited for integration into multi-point data acquisition systems analyzing spatiotemporal variability inside livestock and poultry housing. The uncertainty analysis presented here establishes the framework for performing and determining the uncertainty associated with similar measurement systems.

# 5 Acknowledgments

This research was supported with funding provided by the Iowa Pork Producers Association under NPB Project 14-242. The authors would like to acknowledge the contributions of undergraduate student Grant Hoppes during the preparation and completion of this work.

The research work of Yun Gao was partly supported by the Fundamental Research Funds for the Central Universities of China (2013PY052).

# 6 References

Abdel-Rahman, A., Tropea, C., Slawson, P., & Strong, A. (1987). On temperature compensation in hot-wire anemometry. *Journal of Physics E: Scientific Instruments*, *20*(3), 315.

Al-Garni, A. M. (2007). Low speed calibration of hot-wire anemometers. *Flow Measurement and Instrumentation*, *18*(2), 95–98.

ASHRAE. (2013). *Handbook of fundamentals*. Atlanta, GA: America Society of Heating, Refrigeration and Air Conditioning Engineers.

Aydin, M., & Leutheusser, H. J. (1980). Very low velocity calibration and application of hot-wire probes. *DISA Information*, *1*, 17.

Barfield, B. J., & Henson, W. H. (1971). Calibration of hot-wire and hot-film probes. *Transactions of the ASAE*, *14*(6), 1100–1102. http://doi.org/10.13031/2013.38462

Bowers, C. G., Willits, D. H., & Bowen, H. D. (1988). Comparison of temperature correction methods for hot wire anemometers. *Transactions of the ASAE*, *31*(5), 1552–1555. http://doi.org/10.13031/2013.30899

Bruun, H. H. (1996). Hot-wire anemometry: principles and signal analysis. *Measurement Science*

*and Technology*, *7*(10). Retrieved from http://iopscience.iop.org/0957-0233/7/10/024

Christman, P. J., & Podzimek, J. (1981). Hot-wire anemometer behaviour in low velocity air flow. *Journal of Physics E: Scientific Instruments*, *14*(1), 46.

Collis, D. C., & Williams, M. J. (1959). Two-dimensional convection from heated wires at low Reynolds numbers. *Journal of Fluid Mechanics*, *6*(03), 357–384.

Curtis, S. E. (1983). *Environmental Management in Animal Agriculture*. Ames, IA: The Iowa State University Press.

DeShazer, J. A., Hahn, L., & Xin, H. (2009). Chapter 1: Basic Principles of the Thermal Environment and Livestock Engergetics. In James A. DeShazer, *Livestock Energetics and Thermal Environment Management* (1st ed., pp. 1–22). St. Joseph, MI: American Society of Agricultural and Biological Engineers.

Fox, R. W., McDonald, A. T., & Pritchard, P. J. (1985). *Introduction to fluid mechanics* (Vol. 7). John Wiley & Sons New York.

Heber, A. J., & Boon, C. R. (1993). Air velocity characteristics in an experimental livestock building with nonisothermal jet ventilation. *ASHRAE, ATLANTA, GA(USA).*, (139-1151).

Hillman, P. E. (2009). Chapter 2: Thermoregulatory Physiology. In J. A., DeShazer, *Livestock Energetics and Thermal Environment Management* (1st ed., pp. 23–48). St. Joseph, MI: American Society of Agricultural and Biological Engineers.

Hoge, H. J. (1988). Useful procedure in least squares, and tests of some equations for thermistors. *Review of Scientific Instruments*, *59*(6), 975–979. http://doi.org/10.1063/1.1139762

Hultmark, M., & Smits, A. J. (2010). Temperature corrections for constant temperature and constant current hot-wire anemometers. *Measurement Science and Technology*, *21*(10), 105404.

JCGM. (2008). *Evaluation of measurement data - Guide to the expression of uncertainty in measurement* (First). Geneva, Switzerland: Working Group 1 of the Joint Committee for Guides in Metrology (JCGM/WG 1).

Jerez, S. B., Wang, X., & Zhang, Y. (2014). Quantification of ventilation effectiveness for air quality control in animal buildings. *ASHRAE Transactions*, *120*(1), 460–468.

Kannuluik, W. G., & Carman, E. H. (1951). The temperature dependence of the thermal conductivity of air. *Australian Journal of Chemistry*, *4*(3), 305–314.

Luck, B. D., Davis, J. D., Purswell, J. L., Kiess, A. S., Hoff, S. J., & Olsen, J. W. (2014). Effect of

Measurement Density on Characterizing Air Velocity Distribution in Commercial Broiler Houses. *Transactions of the ASABE*, *57*(5), 1443–1454.

Matlab. (2015). (Version R2015a). MathWorks.

Mori, Y., Imabayashi, M., Hijikata, K., & Yoshida, Y. (1968). Unsteady Heat and Mass Transfer from Small Bodies (1st Report, Spherical Bodies). *The Japan Society of Mechanical Engineers*, *11*(43), 193.

Mount, L. E. (1975). The assessment of thermal environment in relation to pig production. *Livestock Production Science*, *2*(4), 381–392. http://doi.org/10.1016/0301-6226(75)90121-9

Popiolek, Z., Jørgensen, F. E., Melikov, A. K., Silva, M. C. G., & Kierat, W. (2007). Assessment of uncertainty in measurements with low velocity thermal anemometers. *International Journal of Ventilation*, *6*(2), 113–128.

Ramirez, B. C., Hoff, S. J., Gao, Y., & Harmon, J. D. (2015). Commissioning of a novel animal thermal environment replication and measurement system. In *2015 ASABE Annual International Meeting* (p. 1). American Society of Agricultural and Biological Engineers.

Rumyantsev, A. V., & Kharyukov, V. G. (2011). The characteristic size of a sphere in convective heat transfer. *Measurement Techniques*, *54*(5), 524–528.

Schiretz, H. (2012). *The Modern Devices wind speed sensor*. Greelong, Victoria , Austraila: Deakin University.

Skinner, A. J., & Lambert, M. F. (2009). Evaluation of a warm-thermistor flow sensor for use in automatic seepage meters. *Sensors Journal, IEEE*, *9*(9), 1058–1067.

Straw, B. E., Zimmerman, J. J., D'Allaire, S., & Taylor, D. J. (1999). *Disease of swine*. Ames, Iowa: Iowa State Press.

Taylor, B. N., & Kuyatt, C. E. (1994). *Guidelines for evaluating and expressing the uncertainty of NIST measurement results*. Gaithersburg, MD: US Department of Commerce, Technology Administration, National Institute of Standards and Technology.

Yue, Z., & Malmström, T. G. (1998). A simple method for low-speed hot-wire anemometer calibration. *Measurement Science and Technology*, *9*(9), 1506.

Zhang, Y., Barber, E. M., & Ogilvie, J. R. (1988). Simulation of the dynamic thermal environment in a swine barn. *American Society of Agricultural Engineers*.